Ma, X., Huete, A., Moran, S., Ponce-Campos, G., & Eamus, D. (2015). Abrupt shifts in phenology and vegetation productivity under climate extremes. *Journal of Geophysical Research: Biogeosciences*, 120(10), 2036-2052. http://doi.org/10.1002/2015JG003144

Abrupt shifts in phenology and vegetation productivity under climate extremes

Xuanlong Ma*[1], Alfredo Huete[1], Susan Moran[2], Guillermo Ponce-Campos[2], Derek Eamus[3]

[1]Plant Functional Biology & Climate Change Cluster, University of Technology Sydney, Broadway, NSW, 2007 Australia.

[2]USDA Agricultural Research Service, Southwest Watershed Research Center, Tucson, Arizona, 85719 USA.

[3]School of Life Science, University of Technology Sydney, Broadway, NSW, 2007 Australia.

Correspondence to: X. Ma, PO BOX 123, Broadway, NSW, Australia, 2007. (xuanlong.ma@uts.edu.au)

Key Points:

- Climate extremes resulted in abrupt change in phenology and productivity
- Ecosystem sensitivity to hydroclimatic variations peaked in semi-arid regions
- Drying trend in semi-arid ecosystems will result in loss of carbon sink in future

Abstract

Amplification of the hydrologic cycle as a consequence of global warming is predicted to increase climate variability and the frequency and severity of droughts. Recent large-scale drought and flooding over numerous continents provide unique opportunities to understand ecosystem responses to climatic extremes. In this study, we investigated the impacts of the early 21st-century extreme hydroclimatic variations in southeastern Australia on phenology and vegetation productivity using Moderate Resolution Imaging Spectroradiometer Enhanced Vegetation Index and Standardized Precipitation-Evapotranspiration Index. Results revealed dramatic impacts of drought and wet extremes on vegetation dynamics, with abrupt between year changes in phenology. Drought resulted in widespread reductions or collapse in the normal patterns of seasonality such that in many cases there was no detectable phenological cycle during drought years. Across the full-range of biomes examined, we found semi-arid ecosystems to exhibit the largest sensitivity to hydroclimatic variations, exceeding that of arid and humid ecosystems. This result demonstrated the vulnerability of semi-arid ecosystems to climatic extremes and potential loss of ecosystem resilience with future mega-drought events. A skewed distribution of hydroclimatic sensitivity with aridity is of global biogeochemical significance because it suggests current drying trends in semi-arid regions will reduce hydroclimatic sensitivity and suppress the large carbon sink that has been reported during recent wet periods (e.g., 2011 La Niña).

Keywords: climate extremes, carbon cycling, remote sensing, ecological resilience, semi-arid

1. Introduction

Drought has affected most regions of the globe in the early 21st-century, including North America [*Breshears et al.*, 2005; *Ponce-Campos et al.*, 2013], Europe [*Ciais et al.*, 2005; *Reichstein et al.*, 2007; *Ivits et al.*, 2013], the Amazon [*Asner et al.*, 2004], East Asia [*Poulter et al.*, 2013; *Liu et al.*, 2014], and Australia [*van Dijk et al.*, 2013; *Ponce-Campos et al.*, 2013]. In Australia, the recent Millennium Drought, from 2001 until 2009, was the worst on record since 1900 for southeast Australia [*Ummenhofer et al.*, 2009; *Timbal*, 2009] and ended dramatically, with one of the largest La Niña associated wet periods spanning 2010-12. The early 21st-century drought had significant impacts, including significant reduction in agricultural production, reduced water availability for industrial and consumptive use, and increased forest die-back and bushfires [*Semple et al.*, 2010]. Climate model studies show that variability in rainfall is likely to increase under future climate scenarios [*Wetherald & Manabe*, 2002], and the potential for more droughts and greater severity is increasing [*Wang*, 2005].

Amplification of the hydrological cycle as a consequence of global warming increases the frequency, intensity, and spatial extent of extreme climate events globally [*Held & Soden*, 2006; *Sheffield & Wood*, 2008]. The magnitude and direction of the impacts of these extreme climate events on ecosystem function, however, remain largely uncertain, particularly on vegetation phenology and terrestrial primary productivity [*Jentsch et al.*, 2009; *Reichstein et al.*, 2013]. Vegetation dynamics and the phenological metrics derived from ground or remote sensing observations for describing these dynamics, e.g., leaf flush or onset of growing season, are key indicators of ecosystem responses to climate variability and change [*White et al.*, 1997] and these dynamics play an important role in regulating terrestrial carbon and water cycles [*Piao et al.*, 2007; *Richardson et al.*, 2012]. Furthermore, terrestrial primary productivity through photosynthesis is the most fundamental ecosystem function, not only because it provides the fuel that drives all other biological activities, but also due to its significance in locking up carbon in biomass that would otherwise remain in the atmosphere as CO_2 [*Beer et al.*, 2010]. Vegetation phenology and primary productivity together represent key attributes of ecosystems and their shifts under future climate change will have significant impacts on regional and global climate patterns and biogeochemical cycles [*Jones & Cox*, 2005; *Poulter et al.*, 2014].

Understanding vegetation phenology and productivity responses to environmental forcings are of great importance in global change studies that aim to predict how ecosystem function will be impacted by future climate change. Vegetation phenology and productivity responses to climate extremes, however, are complex with variable magnitude and directional responses across seasons, along climatic gradients, and among biomes. In northeastern United States, *Keenan et al.* [2014] observed a strong trend for earlier spring, later autumn and a much larger increase in photosynthetic carbon uptake than increase in respiration under global warming. In the western United States, *Dannenberg et al.* [2014] reported a significant earlier onset of growing season and an enhanced net primary productivity (NPP) associated with El Niño wet conditions compared with La Niña, although the impacts on length of growing season tended to be more complicated. Based on an experimental study conducted over European grasslands, *Jentsch et al.* [2009] found that severe drought and heavy rain events-induced speciesspecific shifts in plant phenology were of the same order of magnitude as one decade of gradual warming.

Although drought is generally associated with declines in vegetation productivity due to water and heat stresses on ecosystem metabolism [*Eamus et al.*, 2013], the magnitude of reduction, which is determined by ecosystem sensitivity to drought, varies dramatically across or even within biomes. While *Liu et al.* [2014] reported that China's national total annual net ecosystem productivity exhibited declines during the period from 2000 to 2011, mainly due to reduction in productivity caused by extensive droughts. *Ivits et al.* [2014] found that drought impacts on ecosystem productivity were not apparent at continental scales in Europe. A recent study conducted over six central United States grassland sites found that sensitivity to drought can vary more than two fold among a single grassland biome [*Knapp et al.*, 2015]. Across southwestern United States grassland, *Moran et al.* [2014] found different responses of vegetation productivity to drought between desert and plains grasslands and shifts in the functional response to inter-annual variations in rainfall due to drought-induced mortality. These findings together highlight the necessity and importance of a comprehensive understanding of the factors that determine the variations in sensitivity to drought across terrestrial biomes.

Recent evidence suggested that Australia, in conjunction with other global semi-arid ecosystems, plays a significant role in the global carbon cycle [*Poulter et al.*, 2014; *Ahlström et al.*, 2015]. Australia, the driest inhabited continent in the world, has an extremely variable climate, with frequent occurrence of widespread drought and wet events. Vegetation phenology and productivity in Australia is highly variable and largely driven by inter-annual variations in rainfall. *Broich et al.* [2014] found rainfall-driven phenological cycles over Australia's large drylands region with the timing of peak greenness varying by over a month between years. Using satellite observations, *Donohue et al*. [2009] found an overall increasing trend of vegetation cover in Australia from 1981 to 2006. Recent drought, however, reduced surface vegetation cover over Australia during the past decade [*Yang et al*., 2014]. In northern Australia's xeric savannas, extreme drought caused substantial tree mortality, which counteracted the net increase in tree cover over past five decades [*Fensham et al*., 2009]. Most recently, *Poulter et al*. [2014] found that Australia contributed to more than half of the exceptional large 2011 global land carbon sink anomaly, and attributed this to one of the strongest La Niña events. Consequently, the extreme variability in climate and high turnover rate of carbon pools in Australia and other global semi-arid ecosystems render these systems an important component of the global carbon cycle [*Poulter et al*., 2014; *Ahlström et al*., 2015].

The objectives of this study were to: (1) investigate shifts in phenology and vegetation productivity across extreme drought and wet years; (2) determine the consequences of contemporary, the early 21st-century climate extremes on ecosystem functioning in southeastern Australia; (3) assess the interactions and relative importance of climatic conditions and vegetation types in determining ecosystem sensitivity and resilience to the impacts of drought. We focused on Australia because it has one of the most variable climates around the globe, and thus it is of interest and importance to know how ecosystems behave under such extreme climate variability. Advances made here will be highly relevant to other water-limited ecosystems around the globe.

2. Data and Methods

2.1 Southeastern Australia study area

Southeastern Australia (SE Australia), is taken to encompass mainland Australia south of 31°S and east of 135°E [*Murphy & Timbal*, 2007]. It is a region of 1.3 million km^2 encompassing all of Victoria, parts of South Australia and New South Wales and including the southern half of the Murray-Darling Basin (Fig. 1). SE Australia represents a large geographical area covering temperate, grassland and desert climates that receives a significant part of annual rainfall in the winter season [*Stern et al.*, 2000]. Within the SE Australia, we defined a ~1200 km long transect originating from the northwest corner (138.5°E 31.1°S) to the southeast corner (149.9°E 31.5°S), passing through a large rainfall-temperature climate gradients, thereby allowing us to investigate directional shifts in phenology and productivity (Fig. 1a). In addition to biogeographic and transect analyses, we also selected six local sites representing major land cover types to gain a better understanding of site-level response of phenology and vegetation productivity to hydroclimatic variations (Fig. 1; Table 2).

The climate pattern of SE Australia is characterized by a transition in precipitation and temperature from the warm-dry northwest inland to the cold-humid southeast coast (Fig. 1). Mean annual precipitation increases steadily from less than 200 mm in the arid interior to > 1400 mm at the coast (Fig. 1b). Annual average daily air temperature (T_{air}) exhibits a decreasing trend from the warm northwest to cooler southeast, with decreases of more than 20°C from the subtropical interior dry lands to less than 10°C at temperate coastal areas (Fig. 1c).

Vegetation within SE Australia was classified into nine major land cover types, including both unmanaged native and managed agricultural vegetation (Table 1). The two most prevalent land cover types within SE Australia are cropland and pasture, covering 20.2% and 18.4% of the land area respectively. These agricultural lands are primarily located within the eastern Murray-Darling-Basin, southern Victoria and regions around Adelaide in South Australia (Fig. 1a, Table 1). Open woodland and hummock grassland, which are the two most prevalent native vegetation types, are primarily located in the northwest semi-arid and arid areas and cover 12.9% and 10.9% land area, respectively. Open forest and closed forests, cover 9.4% and 8.5% of SE Australia, respectively, are primarily located in the eastern coastal and mountain areas where mean annual precipitation is above 1000 mm (Fig. 1a; Table 1). Shrublands are concentrated in the northwest arid interior and cover 7% of SE Australia. Closed forest and shrublands represent the cool-wet end and warm-dry end vegetation types along the rainfall-temperature spectrum within the SE Australia (Fig. 1, Table 1).

2.2 MODIS EVI

Approximately 15 years (February 2000 - Dec 2014) of 16-day 0.05° MODIS Vegetation Indices (MOD13C1, Collection 5) [*Huete et al.*, 2002] were obtained through the online Data Pool at the NASA Land Processes Distributed Active Archive Centre (LP DAAC), USGS/Earth Resources Observation and Science (EROS) Centre (https://lpdaac.usgs.gov). We filtered the original data using the following criteria based on the Quality Control (QC) layers provided along with MOD13C1: (1) corrected product produced at ideal quality for all bands; (2) highest quality for band 1–7; (3) atmospheric correction performed; (4) adjacency correction performed; (5) MOD35 cloud flag indicated "clear"; (6) no cloud-shadow was detected; and (7) low or average aerosol quantities. After filtering out the low-quality observations, the gaps were filled by linearly interpolation using temporally adjacent observations.

The Vegetation Indices are widely used as a proxy of canopy greenness and productivity, an integrative composite property of green leaf area, structure and leaf chlorophyll content [*Myneni & Williams*, 1994]. Vegetation Indices are robust and seamless biophysical measure computed identically across all pixels in time and space regardless of biome type, land cover condition and soil type [*Huete & Glenn*, 2011]. EVI was used as an optimized version of vegetation index that effectively reduces soil background influences and atmospheric noise variations [*Huete et al.*, 2002]. The equation defining EVI is,

$$\mathrm{EVI} = 2.5\frac{\rho_{\mathrm{nir}} - \rho_{\mathrm{red}}}{\rho_{\mathrm{nir}} + 6\rho_{\mathrm{red}} - 7.5\rho_{\mathrm{blue}} + 1} \qquad (1)$$

where ρ_{nir}, ρ_{red} and ρ_{blue} are reflectance of the near infrared (841– 876 nm), red (620–670 nm), and blue (459–479 nm) bands of the MODIS sensor, respectively.

Annual integrated EVI (termed iEVI) have been widely used as a remote sensing measure of annual vegetation productivity from arid grassland to forests [*Holm et al.*, 2003; *Zhang* *et al.*, 2013; Moran et al., 2014], and were found linearly correlated with aboveground net primary productivity [*Ponce-Campos et al.*, 2013]. iEVI was computed as,

$$\mathrm{iEVI} = \sum_{\mathrm{i}=1}^{23} (\mathrm{EVI_i} - \mathrm{EVI_s}) \qquad (2)$$

where EVI_i is MODIS EVI at given date *i*; EVI_s = 0.08 is the soil background signal. iEVI was calculated throughout from January to December for each year (23 MODIS 16-day observations per year).

2.3 Rainfall and temperature datasets

We used monthly gridded rain gauge and temperature datasets provided by the National Climate Centre, Australian Bureau of Meteorology. This meteorology dataset is derived from several thousand ground-station measurements across Australia and the accuracy of these datasets has been assessed through a cross-validation procedure [*Jones et al.*, 2009]. The temperature dataset includes daily maximum temperature (T_{max}, °C) and daily minimum temperature (T_{min}, °C).

2.4 Standardized Precipitation-Evapotranspiration drought Index

We used the global gridded monthly Standardized Precipitation and Evapotranspiration Index (SPEI) provided by digital CSIC (Institutional Repository of the Spanish National Research Council) to characterize drought severity [*Vicente-Serrano et al.*, 2010]. SPEI is a multi-scalar drought index which takes into account both precipitation and temperature to determine drought severity [*Vicente-Serrano et al.*, 2011]. SPEI reflects the cumulative effect of the imbalance between atmospheric supply (precipitation) and demand (potential evapotranspiration). We used SPEI calculated at 3-month time scale considering that shorter time scales are mainly related to soil water content important for plant growth [*Vicente-Serrano et al.*, 2010]. Positive SPEI indicates water-balance greater than historical median, and negative SPEI indicates water-balance less than historical median. Because the SPEI is standardized, wetter and drier climates can be represented in the same way. The original 0.5° data were resampled to 0.05° for analysis with MODIS.

2.5 Land Cover Map

We used the National Dynamic Land Cover Dataset from Geoscience Australia and Bureau of Agricultural and Resource Economics and Sciences (http://www.ga.gov.au/scientific-topics/earth-obs/landcover) [*Lymburner et al.*, 2011] (Fig. 1a; Table 1). This land cover dataset is a nationally consistent and thematically comprehensive land cover classification system for Australia. The accuracy of this dataset has been validated through a comparison with more than 25,000 field sites and show a high degree of consistency with field based information about land cover [*Lymburner et al.*, 2011]. The original 250-m resolution dataset was aggregated to 0.05° to analyze with comparative MODIS and SPEI datasets.

2.6 Aridity Index

To understand the dependency of vegetation response to climatic extremes on the degree of dryness/wetness of the climate at any given location, we calculated the aridity index (AI) for SE Australia using the 14-year BoM meteorological dataset from 2000 to 2013. We used AI instead of mean annual precipitation because AI can better reflect the annual balance between water supply (precipitation) and water demand (potential evapotranspiration) [*Olivier*, 2005]. The AI was calculated as,

$$\mathrm{AI} = \frac{\mathrm{P}}{\mathrm{PET}} \tag{3}$$

where P is annual precipitation (mm); PET is annual potential evapotranspiration (mm), computed using BoM gridded temperature dataset based on the Thornthwaite equation [*Thornthwaite*, 1948]. Classification of AI was according to *UNEP* [1992], which defines "hyper-arid" as AI < 0.03; "arid" as 0.03< AI < 0.2; "semi-arid" as 0.2 < AI < 0.5; "semi-humid" as 0.5 < AI < 0.65; and "humid" as AI > 0.65.

2.7 Extraction of phenological metrics

Four phenological metrics, including the start of growing season (SGS), peak of growing season (PGS), end of growing season (EGS), and length of growing season (LGS), were extracted from the time series of MODIS EVI using an algorithm based on Singular Spectrum Analysis (SSA-Pheno) [*Ma et al.*, 2013] (Fig. 2). The SSA-Pheno algorithm has been described and tested over northern Australia across a wide-range of vegetation structural classes and rainfall regimes and showed robustness and reliability in extracting phenological metrics over highly variable, rainfall-driven ecosystems [*Ma et al.*, 2013]. In this study, SGS was defined as when EVI values equal the minimum value prior to the growing season plus 10% of seasonal amplitude during the green-up phase (Fig. 2). Similarly, EGS was defined as when EVI reaches the value equal to the minimum value after growing season plus 10% of amplitude during the brown-down phase (Fig. 2). PGS is defined as the date when EVI reach maximum value during the growing season (Fig. 2). Finally, LGS was calculated as the difference between EGS and SGS (Fig. 2).

2.8 Statistics

We calculated standardized anomalies of EVI and iEVI to assess the magnitude of the anomalies in EVI and iEVI, as response to seasonal and inter-annual variations in hydroclimatic conditions across space. Standardized anomalies were calculated by dividing anomalies by the climatological standard deviation:

$$x_{\mathrm{sd}} = \frac{x - \mu}{\sigma} \qquad (4)$$

where x_{sd} can be EVI_{sd} or $iEVI_{\mathrm{sd}}$, which is the standardized anomaly of EVI or iEVI, x is EVI or iEVI at any given date or year, μ and σ are mean and standard deviation of EVI or iEVI over 2000-2013 time period, respectively.

We also calculated a hydroclimatic vegetation sensitivity measure, defined as the change in annual vegetation productivity (iEVI) per unit change in annual average SPEI for any given pixel/site. This is equivalent to the slope of the linear regression between iEVI and

SPEI. Before computing the sensitivity, both iEVI and SPEI were linearly detrended to avoid spurious correlations resulting from trends. In this analysis, data processing, statistical analysis and visualization were performed in R scientific computation environment (version 3.1.2, *R Core Team*, 2014) and associated packages contributed by user community (http://cran.r-project.org).

3. Results

3.1 Characteristics of the early 21st-century climatic variations in southeastern Australia

The early 21st-century warm and dry periods spanning SE Australia were characterized by below average precipitation and anomalously higher temperature, representing significantly altered hydroclimatic conditions (Fig. 3a). Significant warming trend ($p < 0.05$) was identified from 1950 to 2013 (Fig. 3a). Annual precipitation was below the long-term average during the entire 2001-2008 time period (Fig. 3a). Although the trend in annual precipitation for SE Australia from 1950 to 2014 was not significant ($p = 0.11$), the reduction in annual precipitation in the study period was significantly lower than long-term average (Fig. 3a).

The SPEI drought index revealed that SE Australia experienced intensified drought and wet cycles in the early 21st-century, with 2002 and 2006 among two of the three worst droughts since 1950 (Fig. 3b). This warm-dry period was broken, dramatically, by an extreme La Niña event in 2010 with regional average annual precipitation surpassing the long-term average by nearly 250 mm (Fig. 3b). Although 2002 was not the driest year in terms of annual precipitation within 1950-2013 (Fig. 3a), both T_{max} and T_{min} exceeded the long-term average by more than 1°C (Fig. 3a). The substantially higher temperature, which enhanced atmospheric evaporative demand, coupled with below average precipitation in 2002 was unique, and resulted in a strong region-wide drought throughout the entire SE Australia (Fig. 3b).

Spatial patterns in drought frequency and severity are shown in Figure 3c,d, by the number of drought month (SPEI < -0.5) and average SPEI during these drought months. Various ‘hot-spots’, affected by drought more than other areas during the early 21st-century, were identified, including almost all of southern Victoria and southwestern New South Wales (Fig. 3c). Some of these regions experienced drought conditions of more than 80 months in total, within the 2000-2013 period (168 months), or approximately half of the study period in the early 21st-century (Fig. 3c).

3.2 Hydroclimatic impacts on seasonality of vegetation growth

Site-level analysis revealed that drought and wet cycles had considerable impacts on vegetation activity and patterns of vegetation response to hydroclimatic variations (Fig. 4). All six local sites experienced severe and protracted drought throughout 2002 and 2003, as indicated by consecutive negative SPEI lasting for 9 - 14 months (Fig. 4). Dramatic declines in vegetation activity were observed at all other sites during 2002-03, where standardized anomaly of EVI remained negative for more than one year (Fig. 4). The wetter-than-average period of 2010-11 resulted in a pulse in vegetation productivity at varied magnitude among sites, with Acacia shrubland site exhibiting the largest increase in EVI (Fig. 4). Among the six sites, wet sclerophyll forest, mallee woodland, and pasture sites were relatively less affected by the 2002-03 drought, although adverse effects of drought on vegetation activity were still observable, particularly at the pasture site (Fig. 4d - f).

Hydroclimatic variations not only affect vegetation activity, but also altered vegetation phenology, as indicated by the change in shape and magnitude of seasonal EVI profiles (right panels of Fig. 4). For instance, the expected phenological cycles either did not occur or were significantly depressed in magnitude in 2002-03 at Acacia shrubland, hummock grassland, and wheat cropland sites (right panels of Fig. 4). Consequently, the length of growing season at these sites can range from more than 6 months in normal or wet years, to 0 day (i.e., no growing season) during severe drought periods.

3.3 Biogeographic patterns in vegetation phenology and productivity across drought and wet cycles

Region-wide maps were generated to assess spatial patterns and temporal variations in phenology and productivity (iEVI) over SE Australia (Figure 5). Within the 2000-2013 period, 2002 (region-wide average SPEI = -0.80) and 2010 (region-wide average SPEI = 0.80), representing the driest and the wettest years respectively, were selected to illustrate the impacts of climate extremes on vegetation phenology and productivity.

Large-scale contrasting hydroclimatic conditions between 2002 and 2010 were evident with SPEI shifting from -1.5 to +1.5 (Figure 5a,b). The impact of climate extremes on biogeographic patterns of vegetation phenology and productivity was dramatic (Fig. 5c-f). Within the areas that phenology was detectable during both 2002 and 2010, there were increasing trends in LGS over 70% of the area in the wet year (Fig. 5d). Hydroclimatic impact on vegetation productivity is shown on Figure 5e-f. Drought resulted in reduced vegetation productivity across 90% of SE Australia in 2002, of which 56% areas showed a negative anomaly in iEVI larger than one standard deviation (Fig. 5e). By contrast, the large-scale rainfall pulse in 2010 resulted in a positive anomaly of vegetation productivity over 90% areas of the study area, of which 53% showed a positive anomaly larger than one standard deviation (Fig. 5f). Region-wide averaged productivity was reduced by 21% in the 2002 drought year relative to the mean of 2000-2013, and was increased by 20% in the 2010 wet year (Fig. 5e,f).

The most noticeable and unique pattern of the impact of drought on phenology is the absence of detectable phenological cycle over vast areas during 2002 drought year, primarily over the northwestern dry interior with hummock grassland and shrubland as dominant land covers (highlighted by red-rectangles on Fig. 5c,d). Time-series EVI was averaged across the regions where phenology was not detectable in 2002 to examine the drought impact on vegetation seasonality over these dryland ecosystems (Figure 6). In the 2002 drought year, seasonal EVI profiles were reduced to nearly a flat line (EVI $\approx$ 0.1, close to soil background value), contrasted with the enhanced vegetation activity throughout the 2010 wet year (Figure 6).

For pixels in which phenology was detectable during both wet and drought years, there was generally advancing trend in SGS in the wet year (ΔSGS = -25.84±44.82 days), and a slight delaying trend was observed during the drought year (ΔSGS = 9.73±37.86 days) (Fig. 7c, d). The drought year was associated with an advancing trend in PGS (ΔPGS = -19.05±37.65 days) (Fig. 7c,d), although the shift in PGS was relatively small as compared to shifts in SGS between drought and wet years (Fig. 7c, d). The trend in EGS was also subtle, with a slightly delaying trend was detected in wet year (ΔEGS = 3.98±44.59 days) and advancing trend in dry year (ΔEGS =11.60±32.79 days) (Fig. 7g, h). Although drought resulted in only subtle change in LGS (ΔLGS = -1.87±45.88 days), the net effect of shifts in SGS and EGS in wet year resulted in an overall extension of LGS (ΔLGS = 29.81±66.41 days) (Fig. 7i, j).

3.4 Variations in ecosystem sensitivity to hydroclimatic variations among land cover types and across a climate gradient

The above analyses revealed differential responses of ecosystem to drought and wet extremes across space and among land cover types. To further explore the dependency of ecosystem-level sensitivity on biotic and abiotic factors, variations in hydroclimatic sensitivity were extracted for 100 samples from northwestern to southeastern SE Australia (Fig. 8a). The hydroclimatic sensitivity for each pixel was defined as the change in annual vegetation productivity (iEVI) per unit change in SPEI, which is equivalent to the slope of the linear regression model between iEVI and SPEI, using 14 years of data from 2000 to 2013.

It is apparent that changes in hydroclimatic sensitivity were dependent on land cover types, increasing dramatically from the northwestern dry interior (where the vegetation was classified as hummock grassland and shrublands), to open woodland (Fig. 8). Sensitivity peaked in cropland and pastures between 34°S and 36°S, and then declined again in coastal humid woodlands and forests located at the southeast end of SE Australia (Fig. 8b).

To further explore the dependency of hydroclimatic sensitivity on the degree of wetness/dryness of climate at any given location, pixel values were averaged by bin of aridity index (every 0.1 increment) over the entire SE Australia (Fig. 9). A notable unimodal distribution was observed, with hydroclimatic sensitivity peaking within semi-arid region (0.2 < AI < 0.5) (Fig. 9). The pattern of highest sensitivity over semi-arid region remained consistent after excluding pixels from managed agricultural ecosystems (cropland and pasture) (inset panel on Fig. 9). Hydroclimatic sensitivity decreased three times more rapidly from its maximum value at semi-arid region to the arid region, relative to the rate of decline of toward the humid region, reflecting the different rates of shift in productivity sensitivity to hydroclimatic variations of semi-arid ecosystems under wetting or drying trends (Fig. 9).

4. Discussion

4.1 Abrupt shifts in phenology and changes in productivity under climatic extremes

We found dramatic impacts of drought and wet extremes on phenology and vegetation productivity. In contrast to mid- and high-latitude biomes in the Northern Hemisphere that generally have recurrent phenological cycles, driven predominantly by temperature variation, the high inter-annual variations in vegetation phenology and productivity at our study area not only highlighted the extreme climatic variability in Australia, but also revealed a high phenological and functional plasticity of Australia's ecosystems. For instance, vegetation growth can be nearly completely dormant during the extreme drought period, yet still maintain capability to be highly productive when favorable periods arrive. These abilities are essential for them to survive and thrive in such a dry and variable climate. It would be of interest in future studies to assess the limit of phenological and functional plasticity of dryland ecosystems in Australia and other global regions to understand the capacity of these ecosystems to adapt fast enough to survive under the impacts of more frequent and severe drought events.

Our results revealed the fact that phenological and functional responses of ecosystems to inter-annual variations in climate were abrupt rather than gradual. We hereby suggest that the speed and direction of long-term gradual shifts in ecosystem function and structure induced by global climate change effects (e.g., warming and elevated atmospheric CO_2) could be suddenly curtailed, or even reversed, by short-term extreme climatic events. For example, a recent study shows that only a few extreme anomalies explain most of the global inter-annual variation in vegetation productivity [*Zscheischler et al.*, 2014]. The rapid and sudden responses of ecosystems to climate have been found in Australia [*Fensham et al*., 1999, 2009] and other global regions [*Peñuelas et al.*, 2004; *Jentsch et al.*, 2008]. These findings together highlight the need for models to explicitly take into account climate-induced abrupt shifts in phenology and productivity for predicting future ecosystem states, particularly in global semi-arid and arid regions where climate is highly variable and vegetation growth is limited by water-availability.

4.2 Dependence of ecosystem hydroclimatic sensitivity on land cover types and climate conditions

An additional and unique finding of this study is that ecosystem hydroclimatic sensitivity peaked over semi-arid, instead of more water-limited arid ecosystems. This is not expected as biomes with the largest limitation in water-availability were also expected to show the largest sensitivity to hydroclimatic variations [*Huxman et al.*, 2004]. Using data from America and Australia, the sensitivity of aboveground net primary production to inter-annual variations in rainfall peaked at the driest sites, and the lowest sensitivity was found at the most mesic sites [*Ponce-Campos et al.*, 2013; *Huxman et al.*, 2004]. A recent study conducted across six central U.S. grassland sites also found that sensitivity of productivity to drought was inversely related to mean annual precipitation [*Knapp et al.*, 2015]. Our results partially agree with these studies, as both reported low hydroclimatic sensitivity of vegetation productivity over humid ecosystems. However, our finding of the maximum sensitivity in semi-arid ecosystems, and much lower sensitivity in arid ecosystems, is unique and refines previous studies conducted in North America and

Australia [*Huxman et al.*, 2004; *Ponce-Campos et al.*, 2013; *Knapp et al.*, 2015].

The lower sensitivity of vegetation productivity at arid and humid ecosystems is likely due to different mechanisms. In arid ecosystems, productivity response is intrinsically constrained by meristem density, leaf area and photosynthetic potential [*Knapp & Smith*, 2001], and plant communities that adapt to dry conditions are expected to be more resistant to drought impact [*Grime et al.*, 2000]. By contrast, the sensitivity of productivity to hydroclimatic variations in more humid and productive ecosystems (e.g., forests) is limited by other resources during the wet periods and may not experience serious water-limitation even during the drought periods [*Knapp & Smith*, 2001].

Although based on different methods, our finding agreed well with a study that found high sensitivity of the frequency of negative anomaly in vegetation greenness to extreme precipitation events across global semi-arid and semi-humid regions [*Liu et al.*, 2013]. A recent study suggested that the loss of resilience associated with dieback would probably occur first at ecosystems that are most sensitive to precipitation variability [*Ponce-Campos et al.*, 2013]. Our finding of hydroclimatic sensitivity peaking in semi-arid ecosystems suggest that these systems are most vulnerable to climatic extremes, and are most likely to experience severe loss of ecosystem resilience with future mega-drought events.

4.3 A skewed distribution of hydroclimatic sensitivity across aridity gradient

The skewed distribution of hydroclimatic sensitivity along the aridity gradient, i.e., rapid decline in sensitivity from the maximum sensitivity in semi-arid region towards minimum sensitivity in arid region is very intriguing and important (Fig. 9). This implies that shifts of the climate in semi-arid regions to drier conditions will lead to rapid decay of sensitivity of productivity to hydroclimatic variations in these ecosystems.

Since 1970s, an overall drying trend in Southern Hemisphere semi-arid regions has been noted (since 1950s for SE Australia, *Cai & Cowan*, 2013) coinciding with a pole-ward expansion of the subtropical dry zone that is partially attributable to anthropogenic climate change [*Cai et al.*, 2012]. This raises an important question of global biogeochemical significance: as to whether the large, terrestrial carbon sink noted in 2011 [*Poulter et al.*, 2014], of which a significant fraction was apportioned to arid and semi-arid regions of Australia, can be repeated with future hydroclimatic wet pulses if semi-arid regions continue their shift to a drier climate?

5. Summary

We have shown that recent climate extremes exerted dramatic impacts on terrestrial ecosystems in southeastern Australia during the early 21st-century, with abrupt change in phenology and vegetation productivity between wet and drought years. Ecosystem hydroclimatic sensitivity varied substantially across space, with maximum sensitivity found at semi-arid ecosystems, demonstrating these ecosystems to be most vulnerable to climatic extremes and susceptible to severe loss of ecosystem resilience with future mega-drought events. Recognition of the dependency of ecosystem responses to hydroclimatic variations on biotic and abiotic factors is thus of critical importance to accurately predict the impacts of future climate change on ecosystem function, and our results suggest that improved models that consider varying hydroclimatic sensitivities among biomes are highly needed.

Acknowledgement

This study was jointly supported by the Australian Research Council - Discovery Project "*Impacts of extreme hydro-meteorological conditions on ecosystem functioning and productivity patterns across Australia*" (ARC-DP140102698, Huete CI), the NASA SMAP Science Definition Team under agreement 08-SMAPSDT08-0042, and the NASA SMAP Science Team under agreement NNH14AX72I. The data used in this study is freely available upon request from the corresponding author.

REFERENCES

Ahlström, A., Raupach, M. R., Schurgers, G., Smith, B., Arneth, A., Jung, M., et al. (2015). The dominant role of semi-arid ecosystems in the trend and variability of the land CO2 sink, *Science*, *348*(6237), 895–899. DOI: 10.1126/science.aaa1668

Beringer, J. (2014). OzFlux Synthesis. Retrieved from: http://www.ozflux.org.au/meetings/september2014/tuesday/26_Beringer.pdf

Beer, C., Reichstein, M., Tomelleri, E., Ciais, P., Jung, M., Carvalhais, N., et al. (2010). Terrestrial Gross Carbon Dioxide Uptake: Global Distribution and Covariation with Climate. *Science*, *329*(5993), 834–838. DOI: 10.1126/science.1184984

Breshears, D. D., Cobb, N. S., Rich, P. M., Price, K. P., Allen, C. D., Balice, R. G., et al. (2005). Regional vegetation die-off in response to global-change-type drought. *Proceedings of the National Academy of Sciences of the United States of America*, *102*(42), 15144–15148. DOI: 10.1073/pnas.0505734102

Broich, M., Huete, A., Tulbure, M. G., Ma, X., Xin, Q., Paget, M., et al. (2014). Land surface phenological response to decadal climate variability across Australia using satellite remote sensing. *Biogeosciences*, *11*(18), 5181–5198. DOI: 10.5194/bg-11-5181-2014

Cai, W., Cowan, T., & Thatcher, M. (2012). Rainfall reductions over Southern Hemisphere semi-arid regions: the role of subtropical dry zone expansion. *Scientific reports*, *2*. DOI: 10.1038/srep00702

Cai, W., & Cowan, T. (2013). Southeast Australia Autumn Rainfall Reduction: A

Climate-Change-Induced Poleward Shift of Ocean–Atmosphere Circulation. *Journal of Climate*, 26(1), 189–205. DOI: 10.1175/JCLI-D-12-00035.1

Ciais, P., Reichstein, M., Viovy, N., Granier, A., Ogée, J., Allard, V., Aubinet, M., et al. (2005). Europe-wide reduction in primary productivity caused by the heat and drought in 2003. *Nature*, 437(7058), 529–33. DOI: 10.1038/nature03972

Dannenberg, M. P., Song, C., Hwang, T., & Wise, E. K. (2015). Empirical evidence of El Niño–Southern Oscillation influence on land surface phenology and productivity in the western United States. *Remote Sensing of Environment*, *159*, 167–180. DOI: 10.1016/j.rse.2014.11.026

Donohue, R. J., McVicar, T. R., & Roderick, M. L. (2009). Climate-related trends in Australian vegetation cover as inferred from satellite observations, 1981–2006. *Global Change Biology*, *15*(4), 1025–1039. DOI: 10.1111/j.1365-2486.2008.01746.x

Eamus, D., Boulain, N., Cleverly, J., & Breshears, D. D. (2013). Global change-type drought-induced tree mortality: vapor pressure deficit is more important than temperature *per se* in causing decline in tree health. *Ecology and Evolution*, 3(8), 2711–2729. DOI: 10.1002/ece3.664

Fensham, R. J., & Holman, J. E. (1999). Temporal and spatial patterns in drought-related tree dieback in Australian savanna. *Journal of Applied Ecology*, *36*(6), 1035–1050. DOI: 10.1046/j.1365-2664.1999.00460.x

Fensham, R. J., Fairfax, R. J., & Ward, D. P. (2009). Drought-induced tree death in savanna. *Global Change Biology*, *15*(2), 380–387. DOI: 10.1111/j.1365-2486.2008.01718.x

Glenn, E. P., Huete, A. R., Nagler, P. L., & Nelson, S. G. (2008). Relationship Between Remotely-sensed Vegetation Indices, Canopy Attributes and Plant Physiological Processes: What Vegetation Indices Can and Cannot Tell Us About the Landscape. *Sensors*, *8*(4), 2136–2160. DOI: 10.3390/s8042136

Grime, J. P., Brown, V. K., Thompson, K., Masters, G. J., Hillier, S. H., Clarke, I. P., et al. (2000). The Response of Two Contrasting Limestone Grasslands to Simulated Climate Change. *Science*, *289*(5480), 762–765. DOI: 10.1126/science.289.5480.762

Held, I. M., & Soden, B. J. (2006). Robust Responses of the Hydrological Cycle to Global Warming. *Journal of Climate*, *19*(21), 5686–5699. DOI: 10.1175/JCLI3990.1

Holm, A. (2003). The use of time-integrated NOAA NDVI data and rainfall to assess landscape degradation in the arid shrubland of Western Australia. *Remote Sensing of Environment*, 85(2), 145–158. DOI: 10.1016/S0034-4257(02)00199-2

Huete, A., Didan, K., Miura, T., Rodriguez, E. P., Gao, X., & Ferreira, L. G. (2002). Overview of the radiometric and biophysical performance of the MODIS vegetation indices. *Remote Sensing of Environment*, *83*(1–2), 195–213. DOI: 10.1016/S0034-4257(02)00096-2

Huete, A. R., Justice, C. O., & van Leeuwen, W. (1999). MODIS Vegetation Index (MOD 13) Algorithm Theoretical Basis Document (ATBD-MOD-13) version 3. Retrieved from: http://modis.gsfc.nasa.gov/data/atbd/atbd_mod13.pdf

Huxman, T. E., Smith, M. D., Fay, P. A., Knapp, A. K., Shaw, M. R., Loik, M. E., et al. (2004). Convergence across biomes to a common rain-use efficiency. *Nature*, 429(6992), 651–654. DOI: 10.1038/nature02561

Ivits, E., Horion, S., Fensholt, R., & Cherlet, M. (2013). Drought footprint on European ecosystems between 1999 and 2010 assessed by remotely sensed vegetation phenology and productivity. *Global Change Biology*, *20*(2), 581–593. DOI: 10.1111/gcb.12393

Jentsch, A., Kreyling, J., Boettcher-Treschkow, J., & Beierkuhnlein, C. (2009). Beyond gradual warming: extreme weather events alter flower phenology of European grassland and heath species. *Global Change Biology*, 15(4), 837–849. DOI: 10.1111/j.1365-2486.2008.01690.x

Jones DA, Wang W, Fawcett R (2009) High-quality spatial climate data-sets for Australia. *Australian Meteorological and Oceanographic Journal*. 58(4): 233-248.

Keeling, C. D., Chin, J. F. S., & Whorf, T. P. (1996). Increased activity of northern vegetation inferred from atmospheric CO_2 measurements. *Nature*, *382*(6587), 146–149. DOI: 10.1038/382146a0

Keenan, T. F., Gray, J., Friedl, M. A., Toomey, M., Bohrer, G., Hollinger, D. Y., et al. (2014). Net carbon uptake has increased through warming-induced changes in temperate forest phenology, *Nature Climate Change*. 4(7), 598–604. DOI: 10.1038/nclimate2253

Knapp, A. K., & Smith, M. D. (2001). Variation Among Biomes in Temporal Dynamics of Aboveground Primary Production. *Science*, 291(5503), 481–484. DOI: 10.1126/science.291.5503.481

Knapp, A. K., Carroll, C. J. W., Denton, E. M., La Pierre, K. J., Collins, S. L., & Smith, M. D. (2015). Differential sensitivity to regional-scale drought in six central US grasslands. *Oecologia*, 177(4), 949–957. DOI: 10.1007/s00442-015-3233-6

Le Quéré, C., Moriarty, R., Andrew, R. M., Peters, G. P., CIAIS, P., Friedlingstein, P., et al. (2014). *Global carbon budget 2014*. *Earth System Science Data*, 7(2), 521–610. DOI: 10.5194/essd-7-47-2015

Leuning, R., Cleugh, H. A., Zegelin, S. J., & Hughes, D. (2005). Carbon and water fluxes over a temperate Eucalyptus forest and a tropical wet/dry savanna in Australia: measurements and comparison with MODIS remote sensing estimates. *Agricultural and Forest Meteorology*, *129*(3-4), 151–173. DOI: 10.1016/j.agrformet.2004.12.004

Liu, C., & Allan, R. P. (2013). Observed and simulated precipitation responses in wet and dry regions 1850–2100. *Environmental Research Letters*, *8*(3), 034002. DOI: 10.1088/1748-9326/8/3/034002

Liu, G., Liu, H., & Yin, Y. (2013). Global patterns of NDVI-indicated vegetation extremes and their sensitivity to climate extremes. *Environmental Research Letters*, 8(2), 025009. DOI: 10.1088/1748-9326/8/2/025009

Liu, Y., Zhou, Y., Ju, W., Wang, S., Wu, X., He, M., & Zhu, G. (2014). Impacts of droughts on carbon sequestration by China's terrestrial ecosystems from 2000 to 2011. *Biogeosciences*, *11*(10), 2583–2599. DOI: 10.5194/bg-11-2583-2014

Lymburner, L., & Australia, G. (2011). *The National Dynamic Land Cover Dataset*. GeoScience Australia. Canberra, Australia.

Ma, X., Huete, A., Yu, Q., Coupe, N. R., Davies, K., Broich, M., et al. (2013). Spatial patterns and temporal dynamics in savanna vegetation phenology across the North Australian Tropical Transect. *Remote Sensing of Environment*, *139*(0), 97–115. DOI: 10.1016/j.rse.2013.07.030

Moran, M. S., Ponce Campos, G. E., Huete, A., McClaran, M. P., Zhang, Y., Hamerlynck, E. P., et al. (2014). Functional response of U.S. grasslands to the early 21st-century drought. *Ecology*, 95(8), 2121–2133. DOI: 10.1890/13-1687.1

Murphy, B. F., & Timbal, B. (2008). A review of recent climate variability and climate change in southeastern Australia. *International Journal of Climatology*, *28*(7), 859–879. DOI: 10.1002/joc.1627

Myneni, R. B., & Williams, D. L. (1994). On the relationship between FAPAR and NDVI. *Remote Sensing of Environment*, *49*(3), 200–211. DOI: 10.1016/0034-4257(94)90016-7

NVIS (National Vegetation Information System). (2012). Australia’s native vegetation – A summary of Australia’s major vegetation groups.

Oliver, J. E. (Ed.). (2005). *The encyclopedia of world climatology*. Springer Science & Business Media.

Peñuelas, J., Filella, I., Zhang, X., Llorens, L., Ogaya, R., Lloret, F., et al. (2004). Complex spatiotemporal phenological shifts as a response to rainfall changes. *New Phytologist*, 161(3), 837–846. DOI: 10.1111/j.1469-8137.2004.01003.x

Ponce-Campos, G., Moran, M., Huete, A., Zhang, Y., Bresloff, C., Huxman, T., Starks, P. (2013). Ecosystem resilience despite large-scale altered hydroclimatic conditions. *Nature*, 494(7437), 349–52. DOI: 10.1038/nature11836

Poulter, B., Pederson, N., Liu, H., Zhu, Z., D’Arrigo, R., Ciais, P., et al. (2013). Recent trends in Inner Asian forest dynamics to temperature and precipitation indicate high sensitivity to climate change. *Agricultural and Forest Meteorology*, *178–179*(0), 31–45. DOI: 10.1016/j.agrformet.2012.12.006

Poulter, B., Frank, D., Ciais, P., Myneni, R. B., Andela, N., Bi, J., et al. (2014). Contribution of semi-arid ecosystems to interannual variability of the global carbon cycle. *Nature, 509*(7502), 600–603. DOI: 10.1038/nature13376

Reichstein, M., Ciais, P., Papale, D., Valentini, R., Running, S., Viovy, N., et al. (2007). Reduction of ecosystem productivity and respiration during the European summer 2003 climate anomaly: a joint flux tower, remote sensing and modelling analysis. *Global Change Biology*, *13*(3), 634–651. DOI: 10.1111/j.1365-2486.2006.01224.x

Richardson, A. D., Anderson, R. S., Arain, M. A., Barr, A. G., Bohrer, G., Chen, G., et al. (2012). Terrestrial biosphere models need better representation of vegetation phenology: results from the North American Carbon Program Site Synthesis. *Global Change Biology*, 18(2), 566–584. DOI: 10.1111/j.1365-2486.2011.02562.x

Semple, B., Rankin, M., Koen, T., & Geeves, G. (2010). A Note on Tree Deaths during the Current (2001–?) Drought in South-eastern Australia. *Australian Geographer*, *41*(3), 391–401. DOI: 10.1080/00049182.2010.498042

Sheffield, J., & Wood, E. (2008). Projected changes in drought occurrence under future global warming from multi-model, multi-scenario, IPCC AR4 simulations. *Climate Dynamics*, 31(1), 79–105. DOI: 10.1007/s00382-007-0340-z

Stern, H., De Hoedt, G., & Ernst, J. (2000). Objective classification of Australian climates. *Australian Meteorological Magazine*, *49*(2), 87-96.

Thornthwaite, C. W. (1948). An approach toward a rational classification of climate. *Geographical Review*, 38, 55–94.

Ummenhofer, C. C., Gupta, Sen, A., Briggs, P. R., England, M. H., McIntosh, P. C., Meyers, G. A., et al. (2011). Indian and Pacific Ocean Influences on Southeast Australian Drought and Soil Moisture. *Journal of Climate*, *24*(5), 1313–1336. DOI: 10.1175/2010JCLI3475.1

United Nations Environment Program (UNEP) (1992). *World Atlas of Desertification*.

van Dijk, A. I. J. M., Beck, H. E., Crosbie, R. S., de Jeu, R. A. M., Liu, Y. Y., Podger, G. M., et al. (2013). The Millennium Drought in southeast Australia (2001-2009): Natural and human causes and implications for water resources, ecosystems, economy, and society. *Water Resources Research*, *49*(2), 1040–1057. DOI: 10.1002/wrcr.20123

Vicente-Serrano, S. M., Beguería, S., & López-Moreno, J. I. (2010). A Multiscalar Drought Index Sensitive to Global Warming: The Standardized Precipitation Evapotranspiration Index. *Journal of Climate*, 23(7), 1696–1718. DOI: 10.1175/2009JCLI2909.1

Vicente-Serrano, S. M., Gouveia, C., Camarero, J. J., Beguería, S., Trigo, R., López-Moreno, J. I., et al. (2013). Response of vegetation to drought time-scales across global land biomes. *Proceedings of the National Academy of Sciences of the United States of America*, 110(1), 52–57. DOI: 10.1073/pnas.1207068110

Wang, D., Morton, D., Masek, J., Wu, A., Nagol, J., Xiong, X., et al. (2012). Impact of sensor degradation on the MODIS NDVI time series. *Remote Sensing of Environment*, *119*(0), 55–61. DOI: 10.1016/j.rse.2011.12.001

White, M. A., Thornton, P. E., & Running, S. W. (2012). A continental phenology model for monitoring vegetation responses to interannual climatic variability. *Global Biogeochemical Cycles*, *11*(2), 217–234. DOI: 10.1029/97GB00330

Yang, Y., Long, D., Guan, H., Scanlon, B. R., Simmons, C. T., Jiang, L., & Xu, X. (2014). GRACE satellite observed hydrological controls on interannual and seasonal variability in surface greenness over mainland Australia. *Journal of Geophysical Research: Biogeosciences*, *119*(12), 2245–2260. DOI: 10.1002/2014JG002670

Zhang, Y., Susan Moran, M., Nearing, M. A., Ponce Campos, G. E., Huete, A. R., Buda, A. R., et al. (2013). Extreme precipitation patterns and reductions of terrestrial ecosystem production across biomes. *Journal of Geophysical Research: Biogeosciences*, 118(1), 148–157. DOI: 10.1029/2012JG002136

Zhang, Y., Voigt, M., & Liu, H. (2015). Contrasting responses of terrestrial ecosystem production to hot temperature extreme regimes between grassland and forest. *Biogeosciences*, 12(2), 549–556. DOI: 10.5194/bg-12-549-2015

Zscheischler, J., Mahecha, M. D., Buttlar, von, J., Harmeling, S., Jung, M., Rammig, A., et al. (2014). A few extreme events dominate global interannual variability in gross primary production. *Environmental Research Letters*, 9(3), 035001. DOI: 10.1088/1748-9326/9/3/035001

Table 1 Summary of major land cover types in southeast Australia.

Name	**Area (km^2)**	**Percentage (%)**	**MAP (mm yr^{-1})**	**MAT (°C)**
Cropland	262765	20	397	17
Pasture	239025	18	397	15
Closed forest	110794	9	958	15
Open forest	122837	9	807	14
Woodland	168434	13	478	16
Open woodland	86835	7	309	18
Shrubland	91696	7	213	19
Hummock grassland	142248	10	249	19
Tussock grassland	35938	2	293	18

Table 2 Summary of location, elevation, climatology, and land cover for six local sites.

Name	Vegetation	Long. (°E)	Lat. (°S)	Elev. (m)	MAP (mm yr^{-1})	MAT (°C)	Ref.
Tumbarumba	Wet sclerophyll forest	148.152	35.657	1200	1277	10	Leuning et al. (2005)
Riggs Creek	Pasture	145.576	36.650	152	539	16	Beringer et al. (2014)
Warracknabeal	Cropland	140.588	34.003	113	264	18	Hochman et al. (2009)
Chowilla	Mallee woodland	142.335	36.226	64	341	16	Meyer et al., 2015
Broken Hill	Hummock grassland	141.325	31.959	313	275	19	NVIS (2012)
Martins Wells	Acacia shrubland	139.137	31.480	196	205	19	NVIS (2012)

Figure 1

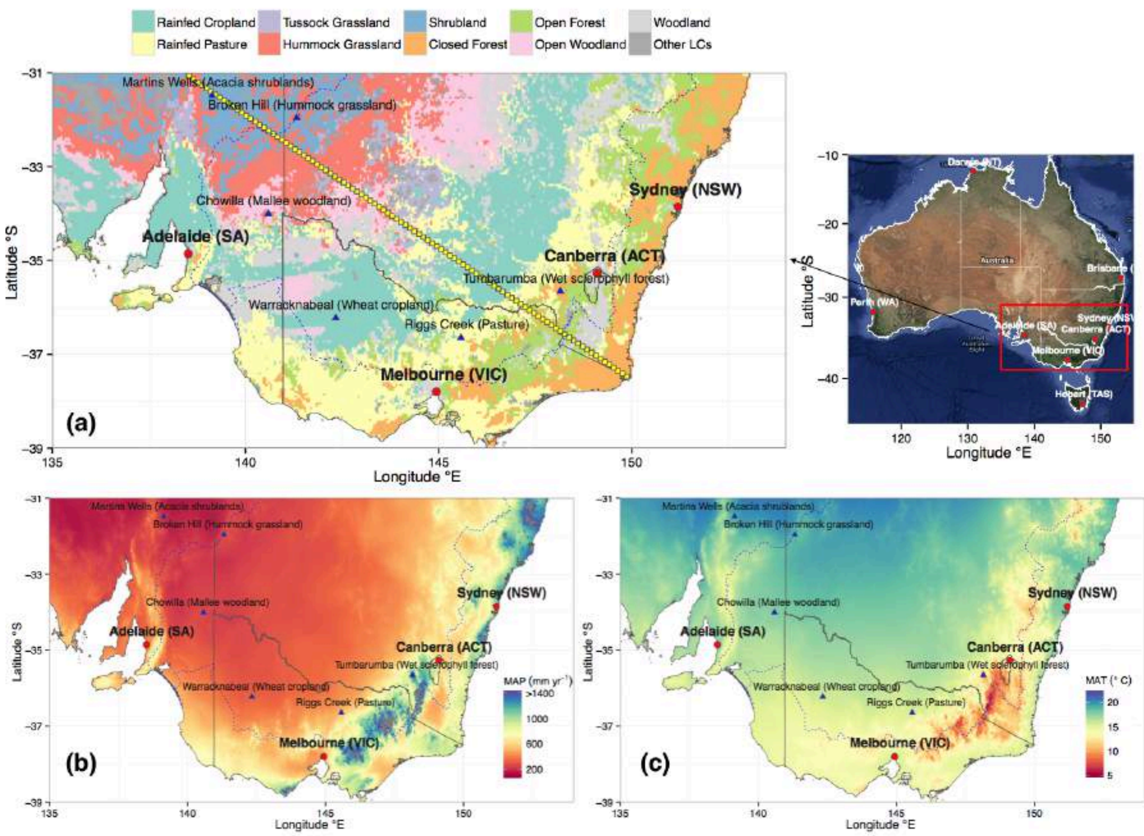

Figure 1 Land cover type and mean climatology of Southeastern Australia. (a) land cover map; (b) mean annual precipitation; (c) mean annual temperature. Solid blue triangles are six local sites that represent different land covers, while solid yellow rectangles indicate ecological-climatological transect from southeast cold-humid coast to northwest warm-dry interior.

Figure 2

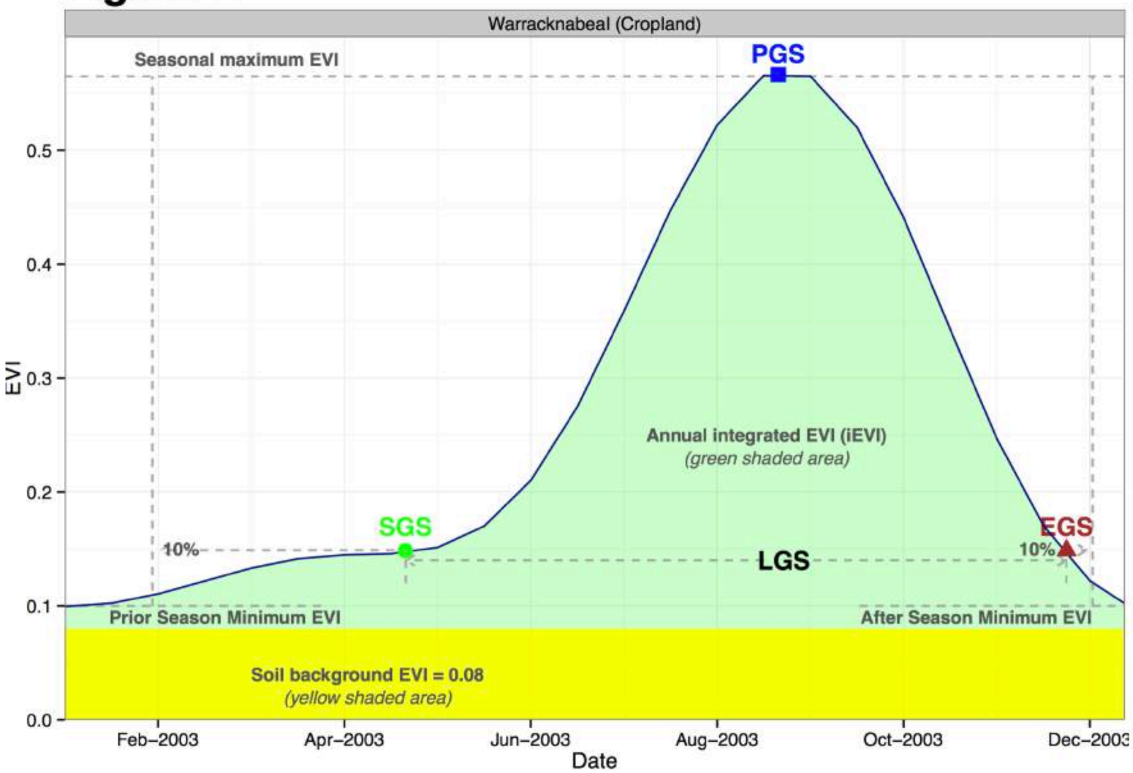

Figure 2 Diagram of algorithm for deriving phenological metrics and annual integrated EVI (iEVI). The diagram uses time series of EVI from Warracknabeal (cropland) site in 2003 for illustration. Key phenological transitional dates, including start of growing season (SGS), peak of growing season (PGS), end of growing season (EGS), as well as length of growing season (LGS = EGS - SGS) are labeled on the diagram. Annual integrated EVI (subtracted soil background signal) is showing as green shaded area. SGS is defined as the timing when EVI is passing the 10% threshold of the seasonal amplitude during green-up phase (seasonal maximum EVI - prior season minimum EVI), and EGS is defined as the timing when EVI is passing the 10% threshold of the seasonal amplitude during brown-down phase (seasonal maximum EVI - after season minimum EVI).

Figure 3

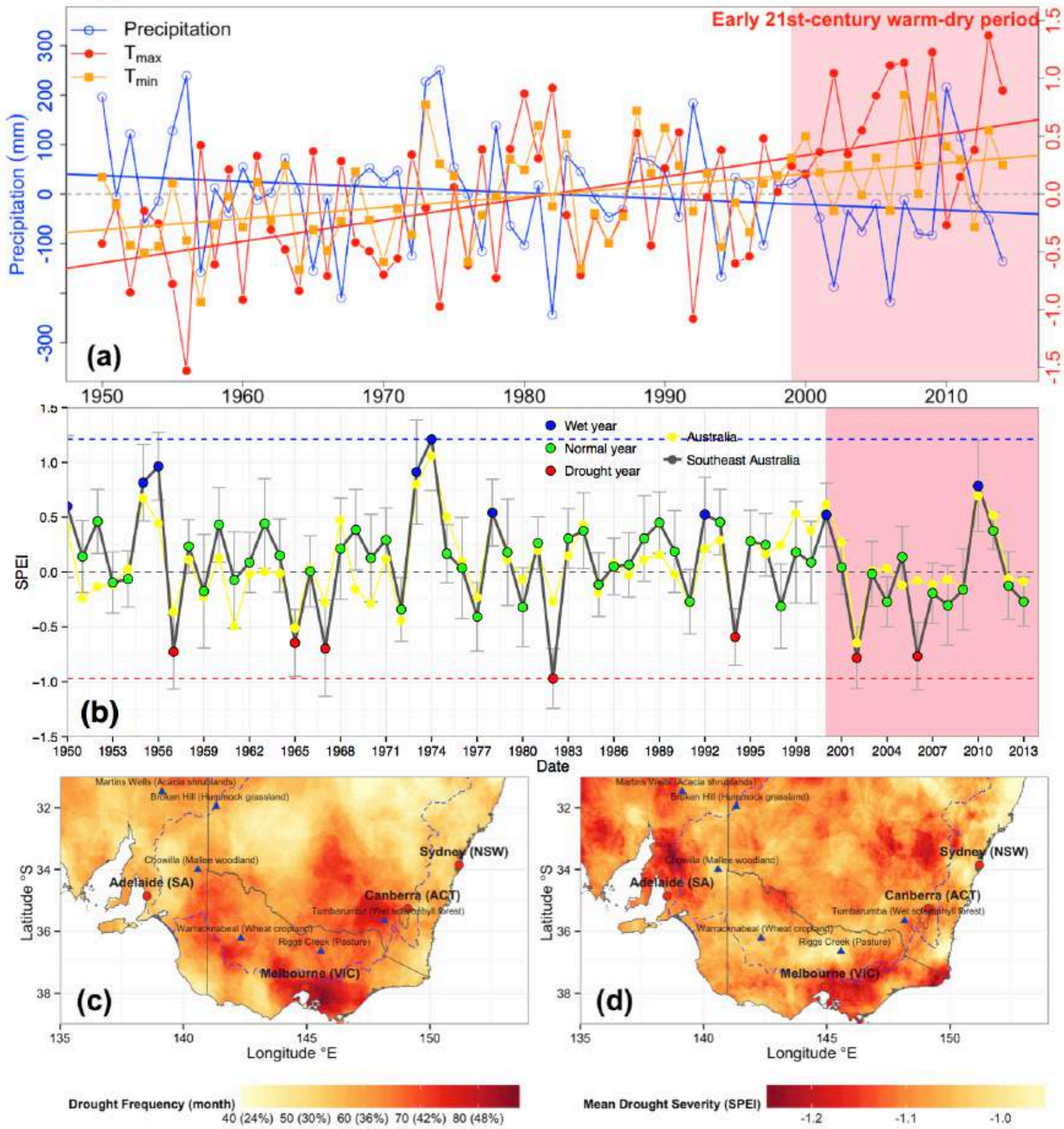

Figure 3 Characteristics of climatology and drought in Southeastern Australia from 1950 to 2014. (a) Region-wide average of annual precipitation anomaly, daily maximum temperature (Tmax) anomaly, and daily minimum temperature (Tmin) anomaly from 1950 to 2014. Solid straight lines indicate the trend lines for each variable; (b) region-wide average annual SPEI over entire Australia (solid yellow line) and SE Australia (solid black line), respectively, from 1950 to 2014; (c) Drought frequency, represented as number of drought months (SPEI < -0.5) during the 2000-2013 time period. Number in bracket is the percentage of drought months regarding 14 years (i.e., number of drought months / 168 months); (d) Mean drought severity, defined as the mean SPEI of drought period (SPEI < -0.5) during 2000-2013.

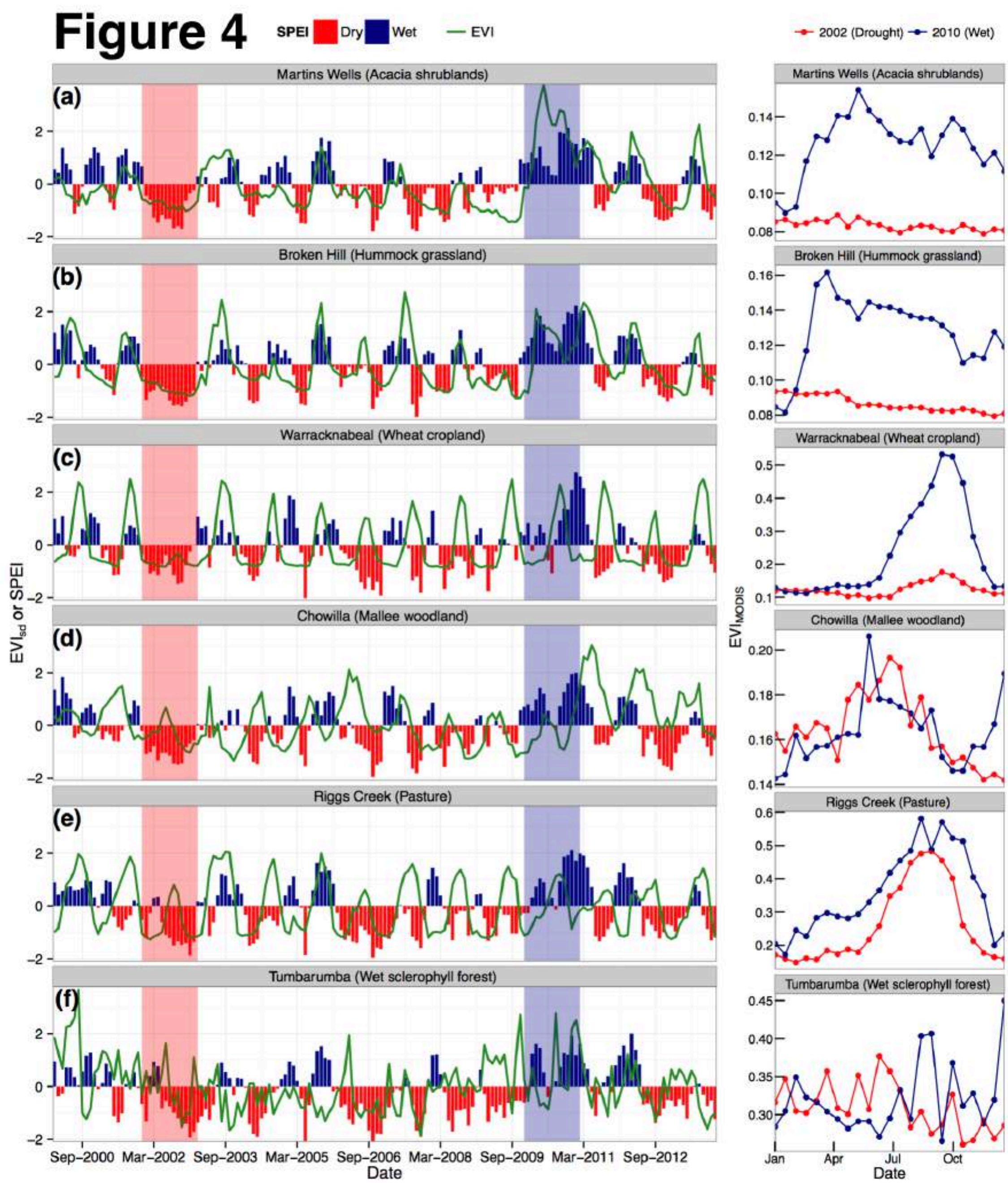

Figure 4 Seasonal and inter-annual variations in EVI and SPEI at six local sites within Southeastern Australia. The solid green line is standardised anomaly of monthly MODIS EVI (EVIsd). Vertical bars are monthly SPEI, with positive SPEI (blue) indicates wet condition and negative SPEI (red) indicates dry condition. Right panels show the seasonal EVI profile during 2002 (drought year) and 2010 (wet year) for each site.

Figure 5

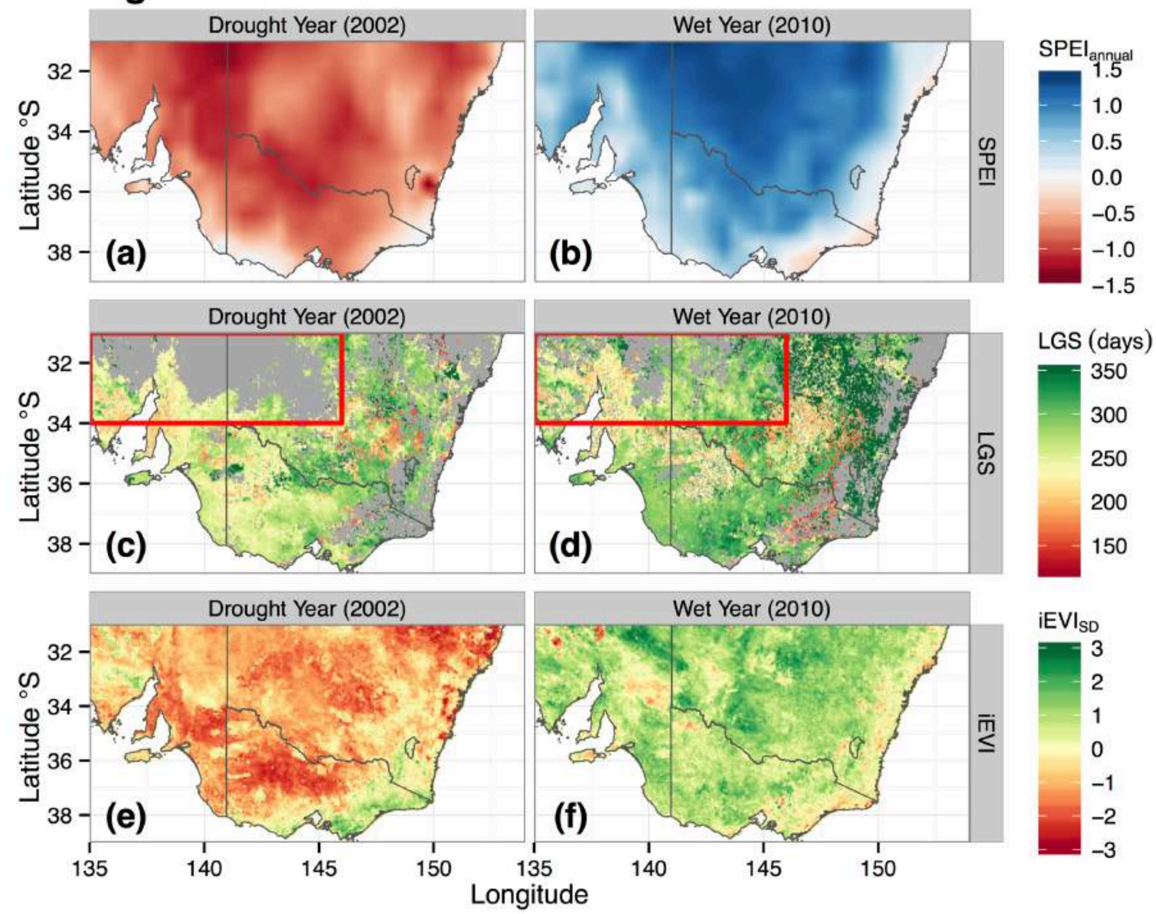

Figure 5 Biogeographical patterns of vegetation phenology and productivity over the SE Australia study area along with SPEI drought index in the driest year (2002) and the wettest year (2010) during the 2000-2013 time period respectively. (a-b) annual mean SPEI; (c-d) length of growing season (LGS); (e-f) standardised anomaly of iEVI (iEVIsd). Grey shaded area indicates the pixels either water-body, or without detectable phenology due to weak seasonality (seasonal EVI amplitude < 0.02). The red-rectangle in panel c, d highlights the regions where phenology over majority of pixels was not detectable during 2002 drought year.

Figure 6

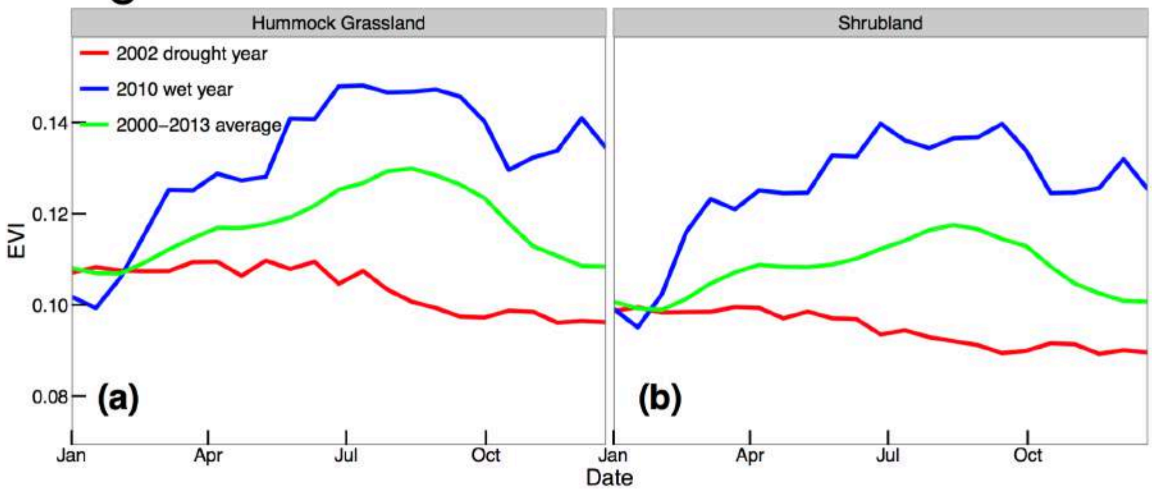

Figure 6 Comparison of hydroclimatic variations-induced shifts in seasonality for hummock grassland and shrubland, respectively. The solid red and blue lines show the EVI profiles for these two vegetation types in 2002 drought and 2010 wet years respectively, while the solid green line shows the climatology average EVI profiles for entire 2000-2014. EVI profiles were averaged using pixels seriously affected by 2002 drought thus no phenology was detected during that year (grey shaded area within the region highlighted by red rectangles on Fig. 5c-d).

Figure 7

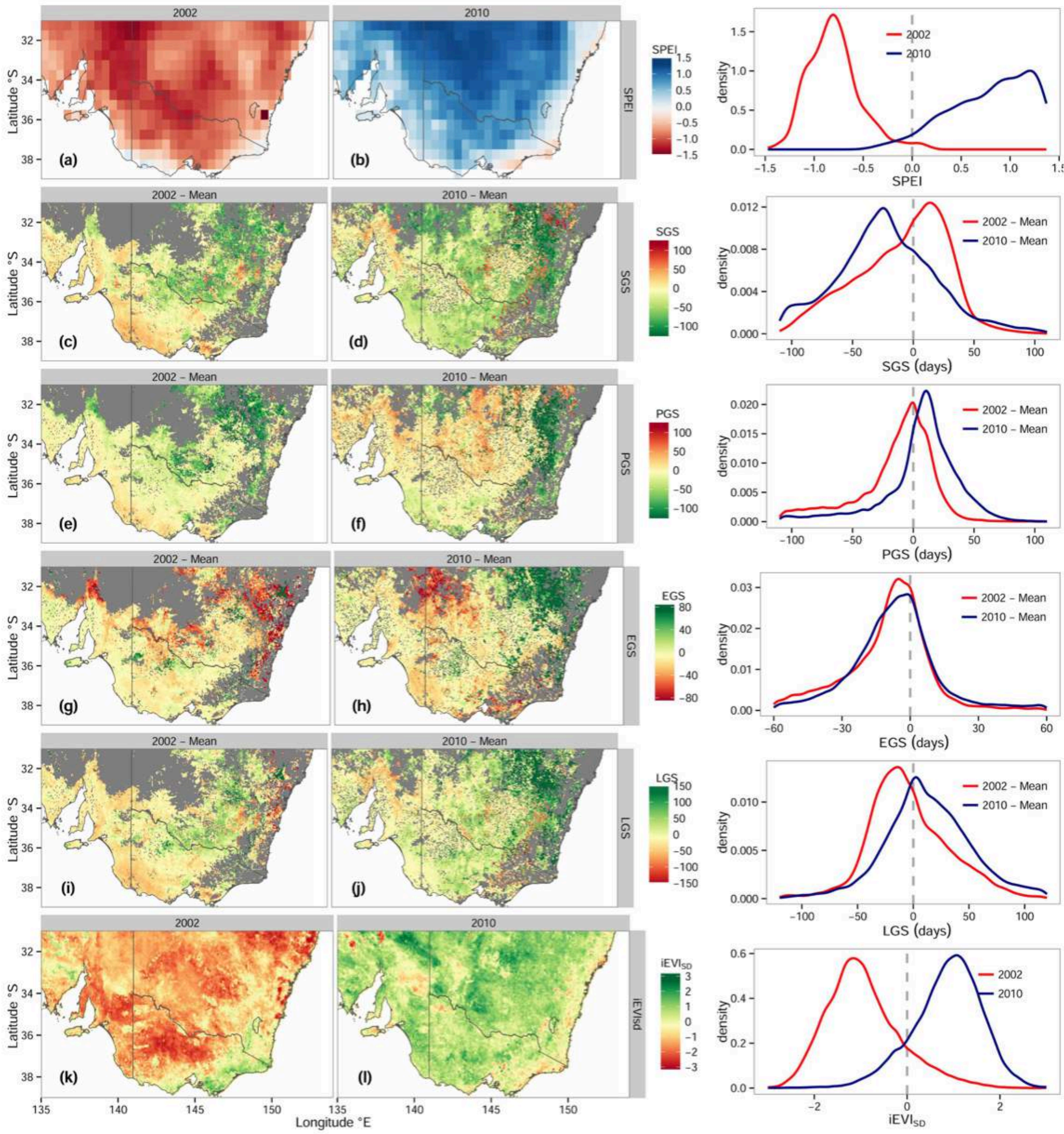

Figure 7 SPEI and anomalies in iEVI and vegetation phenology between 2002-drought year and 2010-wet year, respectively, over the SEA study area. (a-b) SPEI; (c-d) ΔSGS; (e-f) ΔPGS; (g-h) ΔEGS; (i-j) ΔLGS; (k-l) $iEVI_{SD}$ (standardised anomaly of iEVI). For SGS/PGS/EGS, positive difference means delay, and negative difference means advancement, as compared to average of 2000-2013. For each variable, '2002 - Mean' is the difference between values from 2002 and average of entire 2000-2013 time period, and '2010 - Mean' is the difference between value from 2010 and average of entire 2000-2013 time period. Right panels show the empirical probability density function plot of each variable for Δ2002-Mean as well as Δ2010-Mean over the entire SE Australia.

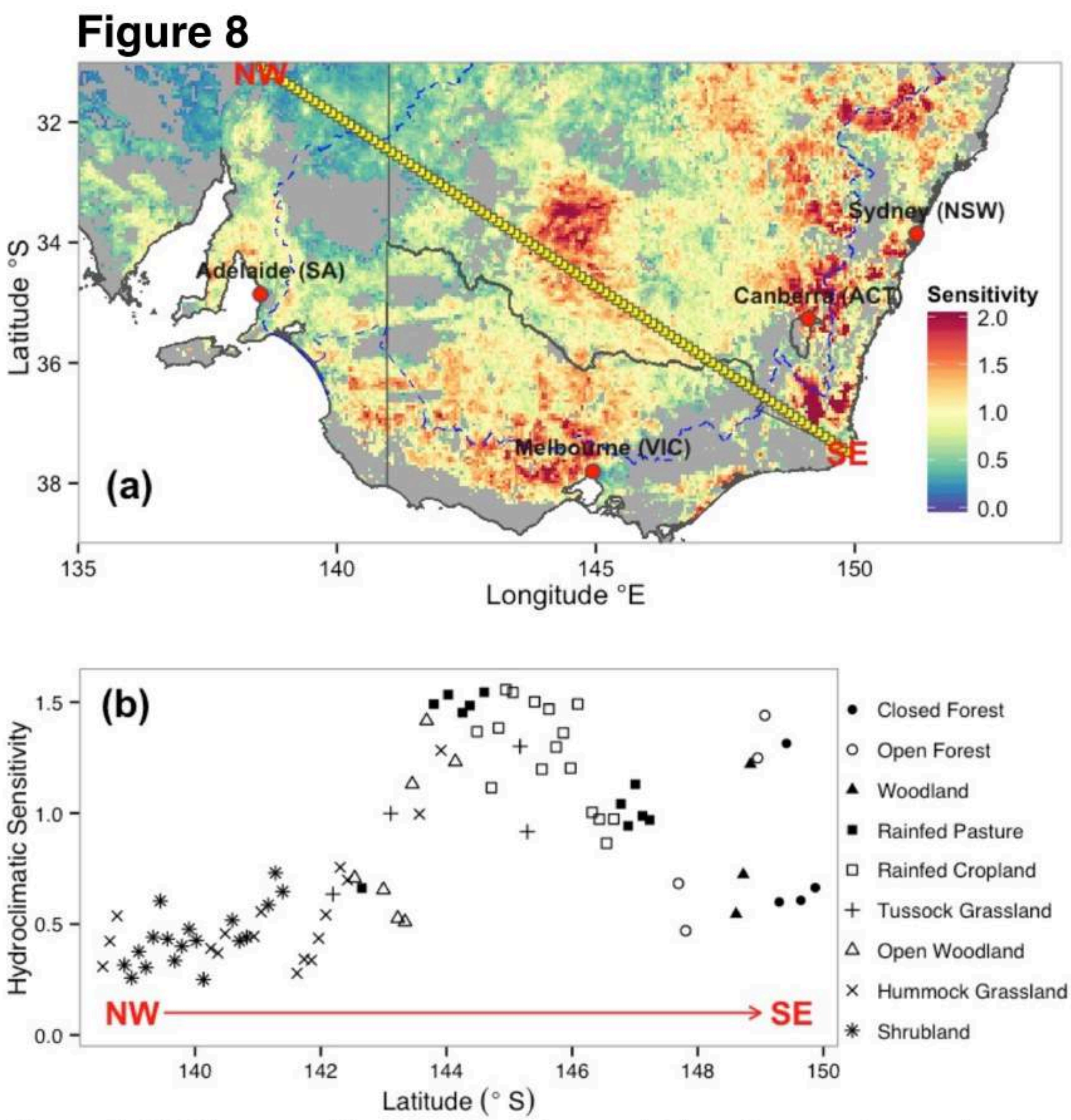

Figure 8 (a) Biogeographic patterns of the sensitivity of vegetation productivity to hydroclimatic variations over SE Australia; (b) change in sensitivity along the transect samples (yellow points on the map, each represents a 0.05°×0.05° pixel) from northwestern SE Australia (138.5°E 31.1°S) to southeastern SE Australia (149.9°E 37.5°S). Grey areas are pixels with no significant relationship between iEVI and SPEI ($p > 0.05$).

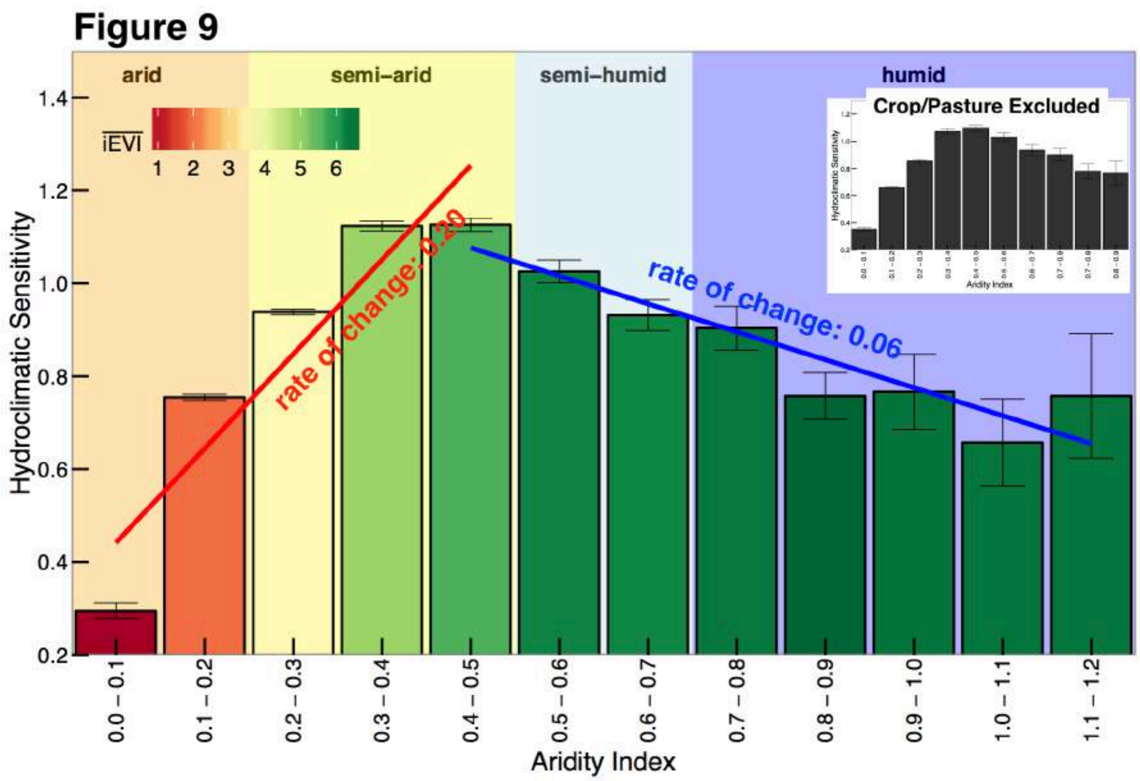

Figure 9 Sensitivity of vegetation productivity to hydroclimatic variations across arid to humid climate regimes. Pixel values over the entire SE Australia study area were averaged by bin (every 0.1 increment) of aridity index (AI). Filled colour bars indicate mean annual vegetation productivity (iEVI) for each AI group. Vertical bars indicate 95% confidential interval of the mean value of hydroclimatic sensitivity. Inset panel shows the same histogram with managed agricultural ecosystems (cropland and pasture) excluded. Solid red and blue lines indicate hydroclimatic sensitivity declines from maximum at semi-arid regions to lower values over arid and humid regions, with the rate of change in sensitivity per unit of AI noted.